Differential Sputtering of Electric Propulsion Grid Material by Ion Bombardment

Rosa Muñoz
Department of Engineering
Colorado State University-Pueblo
Pueblo, CO

Mentors: Dr. John D. Williams and Kirk A. Zoerb
Department of Mechanical Engineering
Colorado State University
Fort Collins, CO

McNair Scholars Summer 2005 Research Program

I. Abstract

Erosion, due to sputtering by energetic ions, of a spacecraft's ion thruster will degrade its performance and eventually lead to its failure. Two important aspects of sputtering by ion bombardment are determination of the number of atoms removed from the surface per impacting ion, and characterization of the directions where sputtered atoms are sent. The purpose of this research project was to explore the second aspect, i.e., the directional (differential) sputtering distributions of atoms removed from materials bombarded by ions formed from inert gases commonly used in electric propulsion devices. Specifically, tests were conducted with titanium, tungsten and tantalum targets that were sputtered by xenon, krypton, and argon ions ranging in energy from 500 eV to 1500 eV. These tests were conducted at several angles of incidence between 0° (corresponding to normal incidence) and 60°. All measurements were performed in a vacuum chamber where a moveable Quartz Crystal Microbalance (QCM) was utilized to obtain differential sputter yield measurements. Graphical representations of the data in a polar format are used to illustrate the sputtering results and comparisons to diffuse (or cosine) emission profiles are made. The goal of this research was to compare the differential sputter yield profiles generated when the ratio between the target atoms mass to the bombarding ion mass was varied. In general, light ions on heavy targets resulted in over cosine behavior, while heavy ions on light targets resulted in under cosine behavior.

Table of Contents

II. Introduction

The following two sections contain background information on electric propulsion and sputtering by energetic ion bombardment.

A. Background of electric propulsion

Electric propulsion can be defined as "The acceleration of gases for the purpose of producing propulsive thrust by electric heating, electric body forces, and/or electric and magnetic body forces" [1]. There are three main categories of electric propulsion including electromagnetic, electrostatic, and electrothermal. The research emphasis at Colorado State University is on electrostatic or ion propulsion, which involves the conversion of electric energy into kinetic energy. The thrust produced by an ion thruster is created by accelerating positive ions through a series of gridded electrodes at one end of the thruster [5]. The beam created by the ion thruster is prevented from being attracted electrically back to the spacecraft by charge and current neutralization of the ion beam using an electron-emitting device called a neutralizer.

Ion propulsion is ideal for spacecraft propulsion because it enables companies to reduce the total amount of propellant needed for a space mission. According to the Boeing Company, less propellant "results in reduced cost for launch, an increase in payload, or an increase in satellite lifetime"[1], and is beneficial not only for the aerospace companies and NASA agencies involved but also for the spacecraft designers and engineers. Electric propulsion systems have a higher specific impulse than chemical propellant systems and over time have shown to be more beneficial spacecraft propulsion systems.

One of the major disadvantages of electric propulsion is the requirement for onboard electrical power to operate the thruster. Typically, kilowatts of power are required to produce relatively low thrusts levels (~40 mN/kW) which require long operational periods to achieve a desired orbit change. Space hardware is difficult or impossible to service during a mission, therefore ion thrusters must be designed to operate for an extensive period of time. Also, electrostatic propulsion systems are designed to produce thrust for an extended period, whereas a chemical rocket exerts thrust all at one time. It is for this reason that I have chosen to do research on the affects of sputtering erosion on the materials used within and nearby ion propulsion systems.

B. Background of Sputtering

The verb sputter comes from the Latin word *sputare* which means to emit saliva with noise. Some other names for sputtering include spluttering and cathode disintegration. It was first described 150 years ago by a man named William Robert Grove and was later elaborated by J. Plüker in 1858. Their first reports explained the affects of vaporization and film formation on metals used for sputtering. Later, in 1897, J.J. Thomson and Rutherford provided the keys for understanding electrons and positive ions in low pressure gas chambers.

Sputtering is defined as the erosion of a surface by energetic particle bombardment (i.e. atoms, ions). Once the atoms have been displaced due to sputtering, they attempt to condense onto (and coat) the surfaces in the vicinity of the sputtered surface. The purpose of our research is to obtain the spatial distribution of the sputtered atoms and to compare our results to previous research on cosine emission

behavior. Sputtering can also be used to apply a protective anti- scratch coating on sunglasses, as well as an ultra-violet finish. Another application of sputtering is applying a gold finish on some gold watches and jewelry. This procedure is completed by sputtering a target of a particular substance with a certain energy to where its atoms are ejected in a certain angle and coat the desired surface.

It is important to clarify the charge exchange process when discussing sputter erosion of ion optics systems used in an ion thruster. Charge exchange can occur whenever neutral atoms (typically moving at a relatively slow velocity) interact with charged particles (typically traveling at a high velocity) and an electron jumps from the neutral atom to the ion thus neutralizing it and giving the neutral atom a charge). When a charge exchange reaction occurs near the negatively biased accelerator grid, the newly formed (slow moving) ion can be drawn into the accelerator grid surface. It has been found that the majority of sputtering occurs "on the inside of the accelerator grid holes, widening the holes during the operation." [6] The location at which the charge exchange ion forms determines the energy, location, and angle of incidence with which it will strike and erode the accelerator grid. The impact of charge exchange ions on the accelerator grid over time sputters the accelerator grid and limits the lifetime of the ion thruster.

The two main types of sputtering that we studied in our research experiment include differential and total sputter yield. Total yield refers to the total number of atoms sputtered per ion striking the target. Differential yield refers to the total amount of atoms per ion sputtered in a certain direction. Differential sputtering is important in electric propulsion because it is necessary to know where the sputtered atoms travel after being displaced. The sputtered atoms will coat the surrounding devices and will affect their performance and limit their lifetime. However, we can not compare our differential yield measurements to the results of others because they have not been recorded but we can compare our total yield measurements. This knowledge will allow engineers to design an ion thruster with an extended lifetime by having more accurate computer models. Cosine distributions are commonly assumed in most wear models of electric propulsion devices and can be explained by the following formula and (Figure 1D):

$$y(\alpha) = \frac{Y \cos(\alpha)}{\pi} \quad . \qquad (1)$$

III. Experimental Methods and Materials

Differential sputter yield testing was performed by first attaching a target to a water-cooled mounting plate in a vacuum system. The vacuum system was then evacuated and baked to ensure the best possible vacuum conditions. No-flow pressures below 7×10^{-6} Torr were achieved before sputter testing was initiated. The basic test apparatus, which is shown schematically in Fig. 1C, includes an ion source equipped with a well-focused, 2.5-cm diameter ion optics system. The ion beam is directed onto the center of the target surface, which is located 23 cm downstream of the ion source grids. This target surface, which is large compared to the beam size, can be rotated to change the angle of incidence of the beam (β). For this study, incidence angles were varied from $\beta=0°$ (normal incidence) to $\beta=60°$.

Sputtered material is sensed as a mass accumulation rate by the quartz crystal monitor (QCM), which is also shown in the Fig. 1C. The QCM operates by measuring

the frequency shifts of the vibrating quartz crystal due to changes in mass. The QCM was mounted on an arm that rotated about the same axis as the one used for target rotation. The QCM sensor swept out an arc that was 17.8 cm in radius and was oriented so its sensing face remained pointed at the midpoint of the ion beam impact zone as suggested in Fig. 1C. Mass accumulation rates were typically measured over the atom ejection angle (α) range from α=-90° to α=+90° relative to the target surface normal vector in 10° increments. The polar angle range from 0° to +90° is referred to as the front half of the hemisphere located above the target, and the range from –90° to 0° is referred to as the back half. Material sputtered in the forward direction (away from the ion beam) is detected in the front half of the hemisphere and material sputtered backward (toward the incident ion beam) is detected in the back half of the hemisphere. It is noted that QCM measurements were not made at positions where the monitor would intercept the ion beam such as 0°.

QCM data were obtained by observing changes in mass on the QCM crystal over prescribed intervals of time (several minutes to tens of minutes) at each position. Data collection was repeated as necessary to assure the mass accumulation rate had reached a stable value before final measurements were recorded. During data collection, the total and partial pressures within the vacuum facility were monitored in nitrogen equivalent units using a residual gas analyzer (RGA).

The total pressure was typically in the 10^{-5} Torr range and the propellant gas was the dominant gas in the chamber at a nitrogen equivalent partial pressure that was very close to the total pressure. Nitrogen (and/or carbon monoxide) was the dominant impurity present during data collection at a partial pressure that was a few percent of the total pressure. Other impurities that were present during data collection were at an order of magnitude lower than partial pressure and included oxygen, water vapor, and hydrogen.

One important concern during sputter yield measurements is the need for dynamically clean target surfaces [9]. This is because the presence of background gases adsorbed onto the target surface can mask the true sputter yield behavior of the material. A particularly troublesome background gas that is known to affect sputter yields of metals is nitrogen, and the presence of oxygen ions and excited neutrals can also affect sputter yield measurements of tungsten and titanium based targets.

Measurements made at various polar angles (α) using the QCM provide mass accumulation rates [R (α)] in gm/sec]. These can be converted into units of atoms/sec by dividing the mass rates by the molecular mass of the sputtered material (M in gm/mol) and multiplying by Avogadro's number (N_A in atoms/mol). These results are converted into fractional sputter yields by dividing by the ion arrival rate, i.e. by the ion current (J) in coul/sec over the ion charge (q) in coul/ion. However, these yields represent only those atoms sputtered onto the QCM sensor through the solid angle subtended by the sensor from the region of beam impact. Because the sensor is swept through a circular arc and its surface always remains normal to the radius vector this solid angle is the same for each measurement.

Assuming the ion impact region is small compared to the arc radius, the solid angle is equal to the sensor area (A_s) divided by the square of the arc radius (r). Dividing the fractional sputter yields by the solid angle subtended by the sensor gives angle-dependent differential sputter yields [y (α)].

The equation [9] for differential sputter yield in atoms/ion/steradian developed as it has been described above is:

$$y(\alpha) = \frac{R(\alpha)\, N_A\, q\, r^2}{M\, J\, A_S} \quad . \qquad (2)$$

The constants needed in Eq. (2) to convert raw rate data [R (α)] into differential yield data for this figure are as follows:

$N_A = 6.023 \times 10^{23}$ atoms/mol
$q = 1.6 \times 10^{-19}$ coul/ion
r = 17.8 cm
M = 12 gm/mol (carbon)
$J = 11 \times 10^{-3}$ coul/sec
$A_s = 0.535$ cm^2

In order to obtain total yield data for non-normal incidence conditions, it would be necessary to measure differential yields over the entire hemisphere above the target [i.e., obtain y (α,ϕ) where ϕ is the azimuthal angle] and then integrate the equation:

$$Y = \int_0^{2\pi} \left(\int_0^{\pi/2} 2\pi \sin(\alpha)\, y(\alpha,\phi)\, d\alpha \right) d\phi \quad . \qquad (3)$$

However, approximate values of the total yields can be obtained from non-normal incidence yield profiles using the far RHS form of Eq. (3) and expressions for each half of the hemisphere located above the target surface. This approximation assumes that the variation in the azimuthal direction varies smoothly between values measured in the plane formed by the target normal and the ion beam. If the differential sputter yield data are curve-fit using Eqs. (4) and (5) for the front and back halves of the hemisphere located above the target, respectively, the total yield can be found analytically using Eq. (6).

$$y(\alpha) = A_5\cos^5(\alpha) + A_4\cos^4(\alpha) + A_3\cos^3(\alpha) + \ldots \ldots A_2\cos^2(\alpha) + A_1\cos(\alpha) \qquad (4)$$

$$y(\alpha) = B_5\cos^5(\alpha) + B_4\cos^4(\alpha) + B_3\cos^3(\alpha) + \ldots \ldots B_2\cos^2(\alpha) + B_1\cos(\alpha) \qquad (5)$$

$$Y = \sum_{n=1}^{5} \frac{\pi}{n+1} A_n + \sum_{n=1}^{5} \frac{\pi}{n+1} B_n \qquad (6)$$

The particles strike the metal target at various angles of incidence and also at different energies ranging from 500 electron volts (eV) to 1500eV. One electron volt corresponds to 1.6 x 10 $^{-19}$ Joules and represents the amount of kinetic energy an ion gains from going through a 1-volt difference in potential. For our experiments, voltages of 500 eV, 750 eV, 1000 eV and 1500 eV were used because this is an important energy range in ion propulsion. It has also been found that the experimental equipment being used malfunctions and shorts when attempting to increase the voltage beyond 1500 eV. Although previous experiments have been done in the research laboratory where materials have been sputtered at voltages in the area of 200eV, it is in the interest of our research to investigate voltages between 500 and 1500eV.

We use the computer program called LabView to obtain our results. It operates by using a series of short programs that are used to communicate between the QCM monitor and a digital multimeter which is used to monitor the ion beam current striking the target. We then use a Microsoft Excel Macro program to plot, curve fit, and integrate the differential yield distributions to obtain the total sputter yield. The measurements acquired from the QCM and

multimeter are used in the mathematical equations described above to determine the differential yield value.

IV. Results

(See Figures 2-10 in Appendix)

V. Discussion

Some of the biggest factors in determining the total yield are atomic mass and the energy of the bombarding ion. For example, the atomic mass of an argon ion is 40 amu, and as it strikes the target, the atoms within it are displaced over a specific volume (typically referred to as the collision cascade volume [3]). This is determined by the target density and atomic mass and also by the ion energy and mass. The mass of the target atom must be taken into account because the efficiency of momentum transfer depends upon the mass of both of the particles. The highest efficiency occurs when the two masses are similar to one another. If the mass of the target atom is several times larger than the propellant atom, the number of sputtered atoms will be decreased significantly. The reason for this being that it is difficult to impart momentum to the target atoms from a collision with a light ion.

Another factor that plays a major role in the total yield is that of the ion energy. If the ion strikes the target at a low energy, it will not sputter very many atoms because it does not have enough energy to initiate or disperse a large volume of disturbed atoms. If an ion strikes a surface at a higher energy however, it initiates a larger collision cascade that increases the probability that more atoms will be sputtered and directed toward the surface.

Our resulting distributions all seem to have a shape similar to those of Wehner in his early 1959 differential yield distributions [7]. For the first set of graphs, argon ions on a tantalum target(Figure 2), I noticed that the peak sputter yield was at 30° and that the graphs approach the cosine distribution curve as the variables such as energy and angle of incidence are increased. It had an awesome curve fit when compared to the total sputter yield measurements from Yamamura and Tawara. It is also important to note that the 750, 1000 and 1500eV total sputter yield graphs were all similar in size and shape. The second set of graphs, krypton ions on a tantalum target (Figure 3), also revealed that the peak sputter yield was at 30° and gave an even better comparison to the results of Yamamura and Tawara. I noticed that the graph that had the greatest sputter yield was that of 1500eV with an incidence angle at 30°. The third set of graphs (Figure 4), xenon ions on a tantalum target revealed a different peak sputter yield at 45°, also at an energy of 1500 eV. When comparing our data to that of Yamamura and Tawara, we observed that three of our data points were in direct relation to theirs, but that one point was independent. We believe that our values are skewed as a result of a power outage during the data collection period; therefore we consider this data point to be questionable.

The fourth table of data (Figure 5), which includes charts of argon ions on a titanium target, was found to have a peak sputter yield at yet another incidence angle at 60 °. The graph that was most closely related to that of a cosine distribution curve was that of 1000eV, where all five plots were relatively spherical in shape. In the fifth table, where the results of krypton ions on a titanium target are shown (Figure 6), a peak sputter yield at 60° was evident. You will notice that the incidence angle plots of

15° will change in shape from cartoid to a more circular shape as the voltage is increased. When comparing our results to those of Yamamura and Tawara, we found some evident discrepancies. There is one point that is directly correlated to their data, and the others are all unrelated to that point and to their results. We are not sure why our data is so different from Yamamura and Tawara's [10] but we are investigating the causes further. One cause may be that titanium is known to react easily with nitrogen; therefore the trace amounts of the element could be directly affecting our results. For the graphs of xenon ions on a titanium target (Figure 7) the peak sputter yield is again at 60°, which disagrees with our deduction that the peak sputter yield should be at 45° for each ion on each target surface. The plotted graphs for 500 and 750eV are very different in shape, where the graph of 750eV gives a larger value for the differential yield. Also, when comparing our results to those of Yamamura and Tawara, they are not related in any sense.

The seventh table of data (Figure 8), argon ions on a tungsten target, shows a peak sputter yield at 45°, where surprisingly the greatest differential yield is achieved at 500eV. When comparing to Yamamura and Tawara's results, we found that our results measured up accordingly. The graphs of krypton ions on a tungsten target (Figure 9) in the eighth table, also show a peak sputter yield at 45° which agrees with our original statement. And once again, our results directly correlate with those of Yamamura and Tawara. In the final graph of xenon ions on a tungsten target (Figure 10), once again the peak sputter yield is at 45°. However, the greatest differential yield is observed at a voltage of 750eV with an incidence angle of 45°.

The differential sputter yield profile was observed to be fairly flat, with a majority of material sputtered at high polar angles. This same behavior was observed with both titanium and tungsten targets and is expected when heavy particles like Xenon are directed at targets comprised of light atoms like titanium.

Cosine distributions are commonly assumed in most wear models of electric propulsion devices. It has been observed that all graphs approach the cosine distribution curve as the variables of voltage and angle of incidence are increased. The cosine distribution curve does not predict what a graph will look like when different energies and incidence angles are applied. It only predicts what will eventually happen to the graphs if particles with high energies are applied. It is for this reason that we would recommend altering the cosine distribution assumptions in many computer models to reflect a distribution resembling the distributions resulting from this study.

VI. Conclusions

The results of our experiments have brought us to some basic conclusions. We have found that the total yield increases as the target angle of incidence increases, and reaches its peak sputter yield at approximately 45°. One can conceptualize this result in the following way. When an ion strikes a target atom at normal incidence, the majority of its momentum and energy gets directly absorbed into the target and minimizes the collision cascade, thus resulting in a low sputter yield. The energy from the ion is directly absorbed into the system to where the target's surface atoms receive the energy and transfer it directly though an elastic collision to the atoms beneath it. However, as the target angle increases, the ion beam is more likely to strike the target at an angle at which the target surface atoms directly affect the

adjacent atoms instead of those directly underneath. These conditions are more preferential to obtain a higher sputter yield.

According to sputtering computer simulations and some experiments done by other researchers [6, 8], the maximum total yield is obtained at 60 or even 70°. A possible explanation for why our peak sputter yield values differ is because the beam area becomes too large on the target at angles larger than 45° and our QCM is only able to measure one specific point on the target surface at a time. The researchers who have achieved a peak sputter yield at angle measurements larger than 45° must have had a measuring device that was able to take more than one mass accumulation amount at a time.

We have established that the QCM method we used to acquire our data is accurate in obtaining total yields at normal incidence when compared to available literature values. The Quartz Crystal Microbalance is ideal for obtaining mass accumulation measurements over an allotted period of time. Other methods of measuring sputtered material such as that recorded in the paper written by Maris Mantenieks [4] were researched but were found to be non-ideal for our research lab set-up. In order to use the semi-cylindrical collector strip in our lab, we would have had to drill holes in the aluminum for every angle of incidence we wanted to study and we would also have to send the sputter collection papers elsewhere for analysis. Also, a laser induced fluorescence (LIF) method [2] was found to be incompatible with our current vacuum system set-up and too costly as well. The QCM method is ideal for our purposes because of the quick results we obtain and because of the relatively low cost involved in operating the system.

When comparing the acquired sputtered graphs, a simulated computer model of a cosine distribution curve was comprised and used. The majority of our results did not resemble the cosine distribution assumed in many sputtering computer simulations. An example of a typical cosine distribution curve (Figure 1D) is shown in the appendix. Our data charts do not fit the cosine distribution curve and we believe that the computer models should be updated to a distribution similar to what we have measured. The majority of our curves are over-cosine, meaning that the cosine distribution curve does not accurately predict the contour or differential yield of the plotted graphs.

VII. References

1. **Boeing Aerospace Website**. http://www.boeing.com/defense-space/space/bss/factsheets/xips/xips.html

2. **Crofton, M.W.**; Murray, J.C.; Pollard, J.E. "Angular Properties of Xe Sputtered Molybdenum at Low Impingement Energy," *The Aerospace Corporation*, 1-6, 2004.

3. **Dolaghan, John Samuel.** "Monte Carlo Simulation of Molecular Redistribution in an Enclosure Due to Sputtering," *Colorado State University*, Thesis, 1991.

4. **Mantenieks, Maris A.**; Foster, John E. "Low Energy Xenon Ion Sputtering Yield Measurements," *27th International Electrical Propulsion Conference*, 1-8, 2001.

5. **Robinson, Raymond S.** "Physical Process in Directed Ion Beam Sputtering," *Colorado State University*, Thesis, 1979.

6. **Tartz, M.; Neumann**, H.; Fritshe, B.; Leiter, H.J.; Esch, J. "Investigation of Sputter Behaviour of Ion Thruster Grid Materials," *American Institute of Aeronautics and Astronautics*, 40th Joint Propulsion Conference and Exhibit, 1-6, 2004.

7. **Wehner, G.K.**; Rosenburg, D. "Angular Distribution of Sputtered Material," *Journal of Applied Physics*, Volume 31, Number 1, 177-179, January 1960.

8. **Wehner, Gottfried.** "Influence of the Angle of Incidence on Sputtering Yields," *Journal of Applied Physics*, Volume 30, Number 11, 1762-1765, November 1959.

9. **Williams, John D.**; Johnson, Mark L.; Williams, Desiree D. "Differential Sputtering Behavior of Pyrolytic Graphite and Carbon-Carbon Composite under Xenon Bombardment," *American Institute of Aeronautics and Astronautics*, 40th Joint Propulsion Conference, 1-21, July 2004.

10. **Yamamura, Yasunori**; Tawara, Hiro. "Energy Dependence of Ion-Induced Sputtering Yields from Monatomic Solids at Normal Incidence," *Atomic Data and Nuclear Data Tables 62*, 1996.

VIII. Appendix

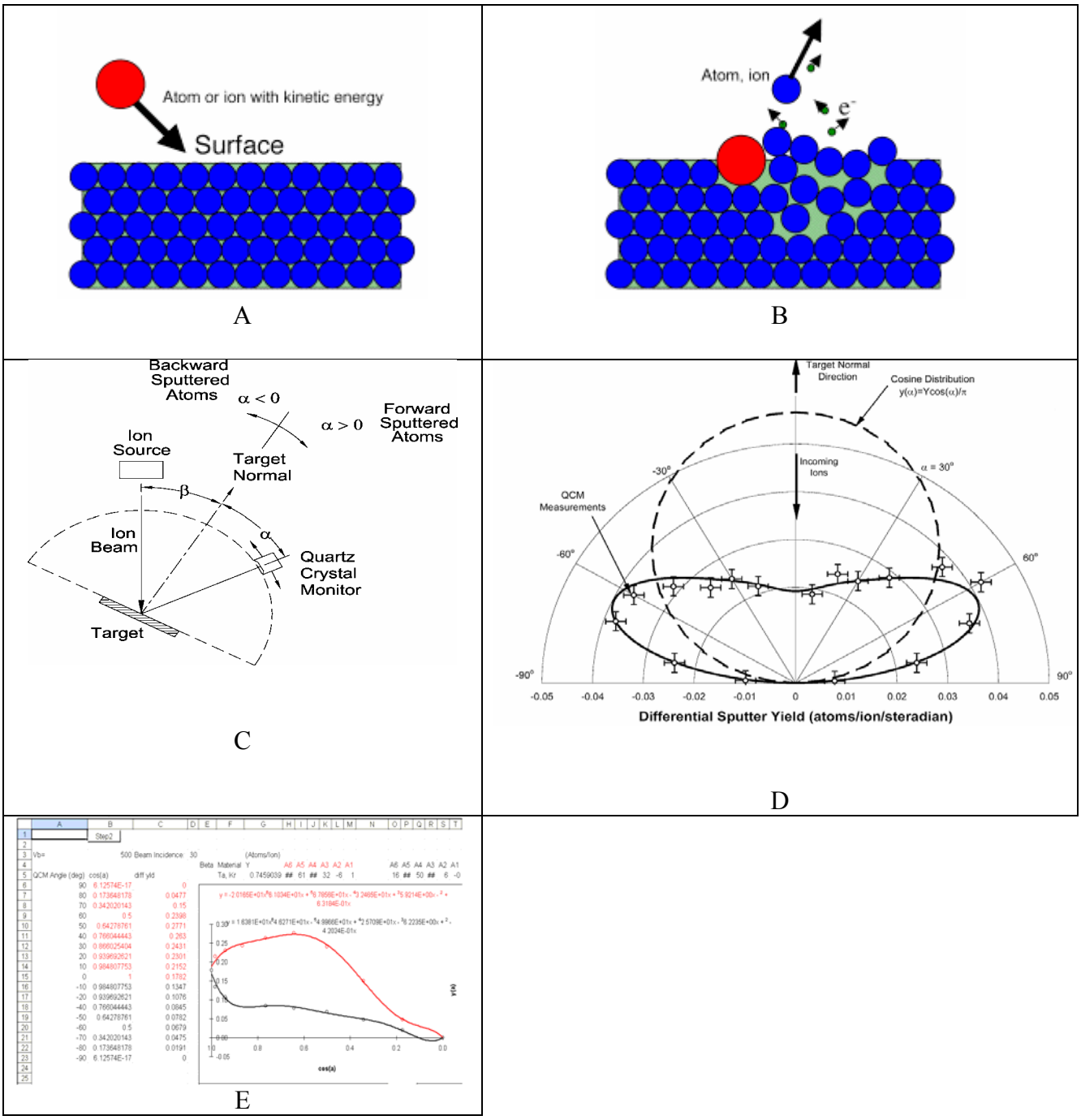

Figure 1A. Ion with certain energy before bombarding the target surface
Figure 1B. Beginning of collision cascade where the ion strikes the target and sputters off ions
Figure 1C. Sketch of our test apparatus
Figure 1D. Typical cosine distribution curve
Figure 1E. Example of typical Excel spreadsheet

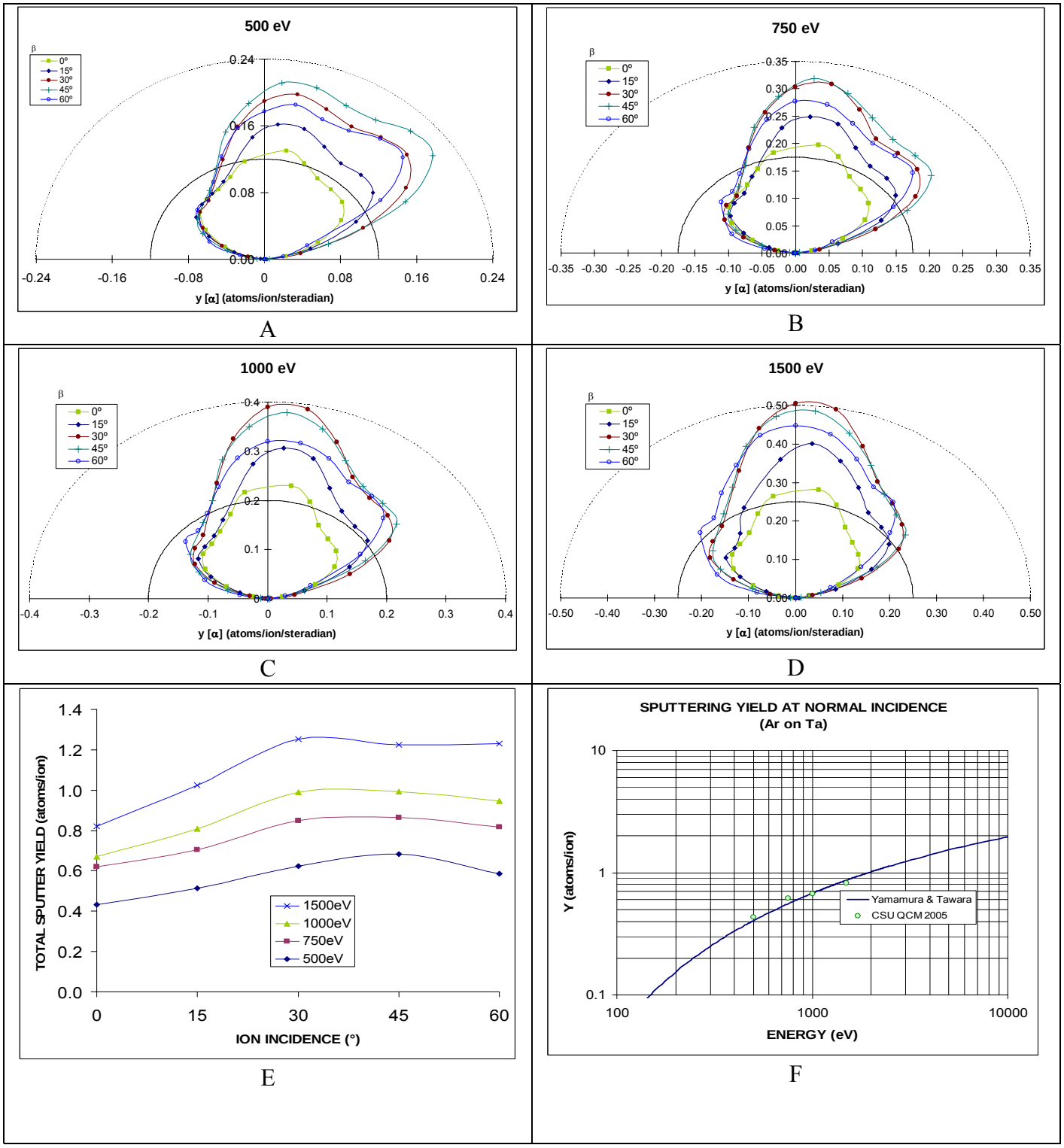

Figure 2. Results of Argon ions on Tantalum target

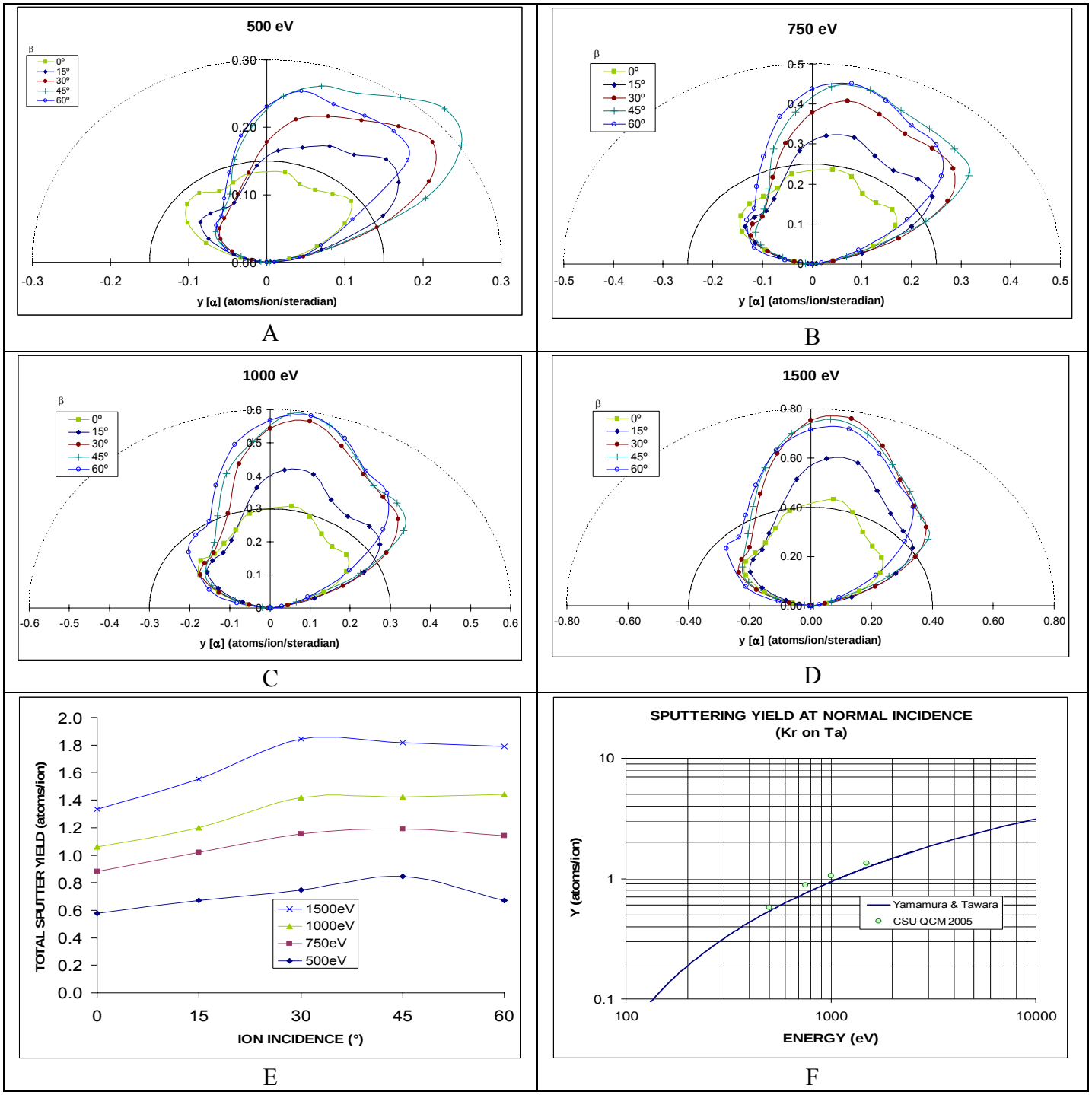

Figure 3. Results of Krypton ions on Tantalum target

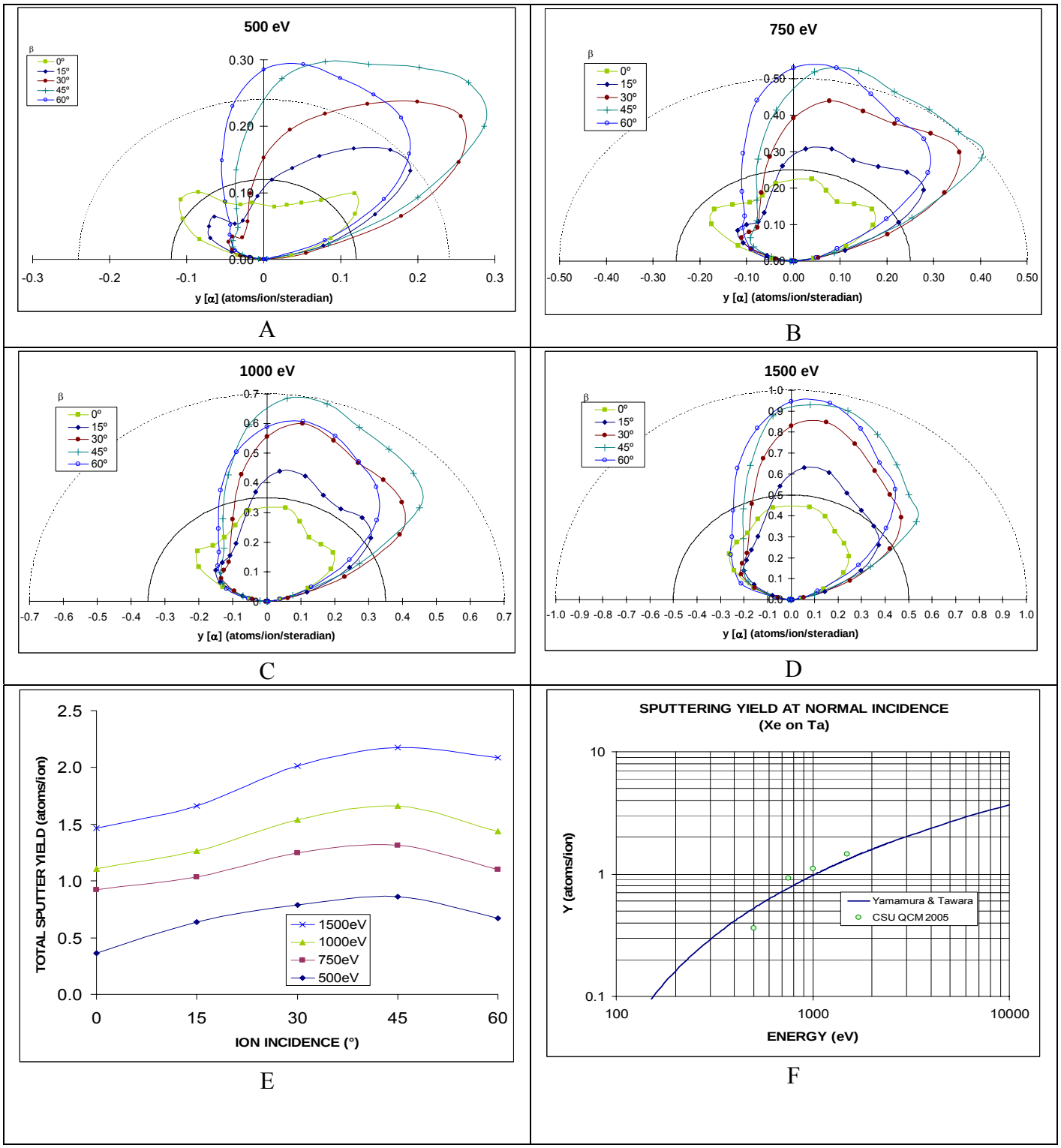

Figure 4. Results of Xenon ions on Tantalum target

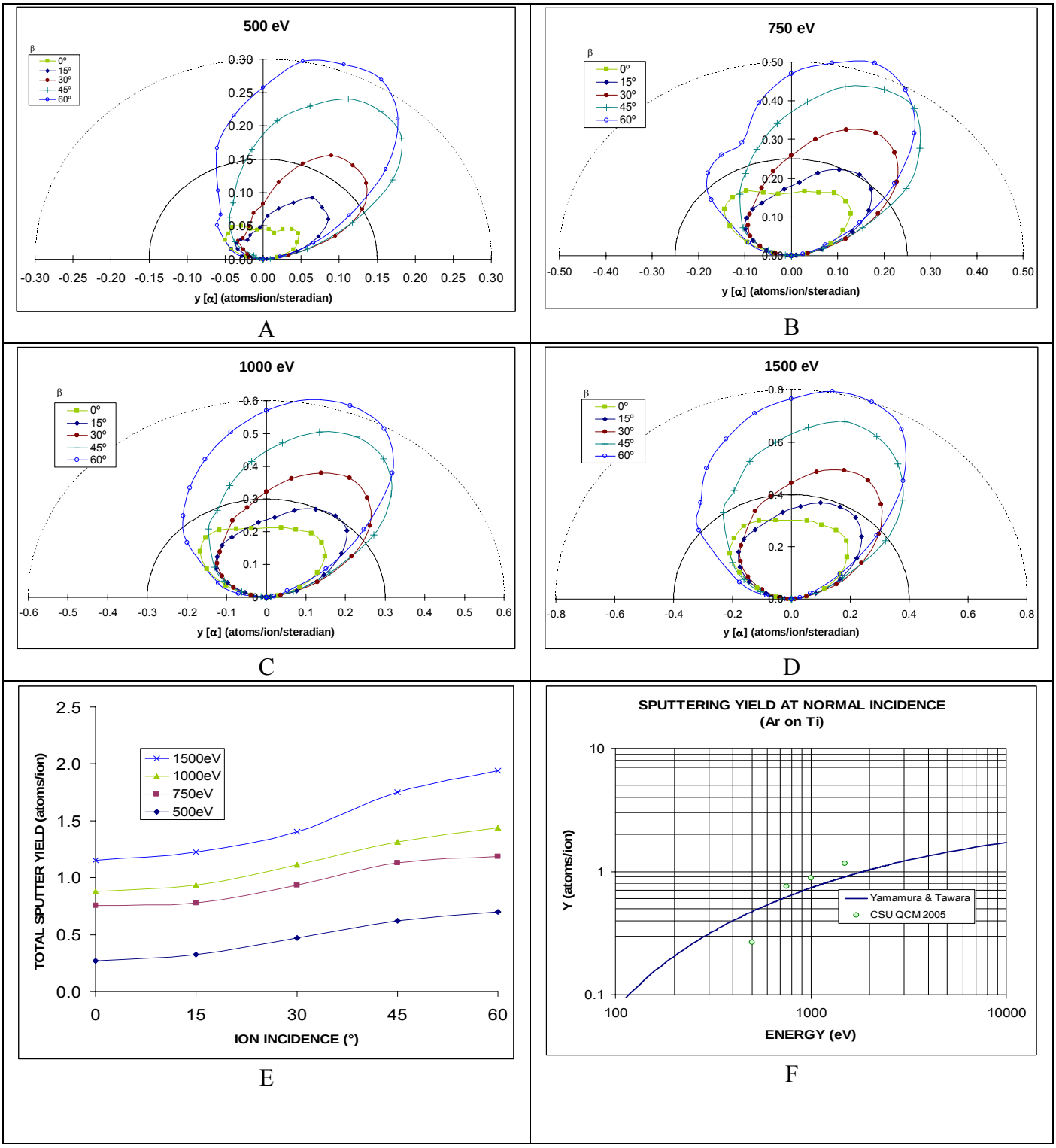

Figure 5. Results of Argon ions on Titanium target

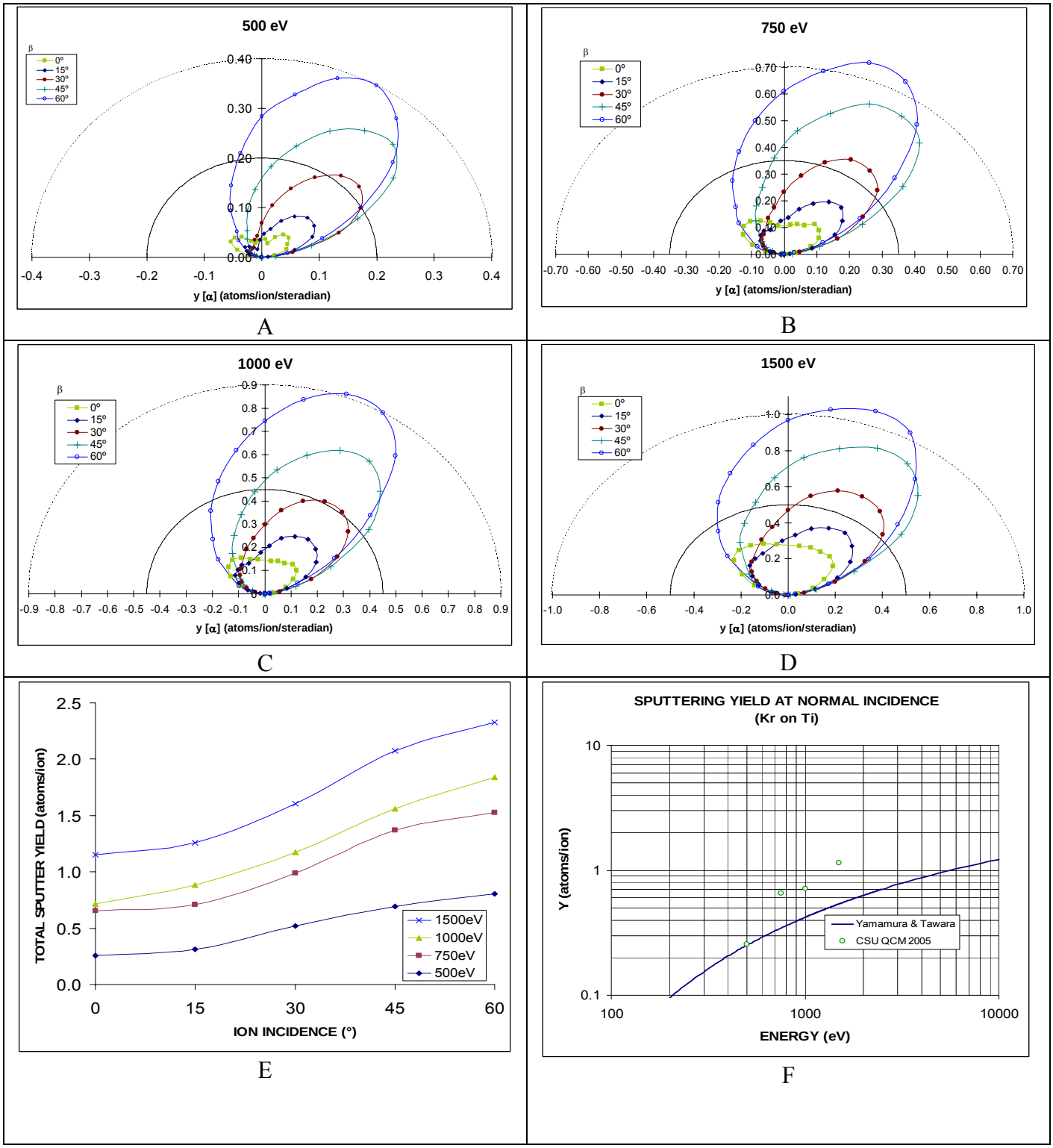

Figure 6. Results of Krypton ions on Titanium target

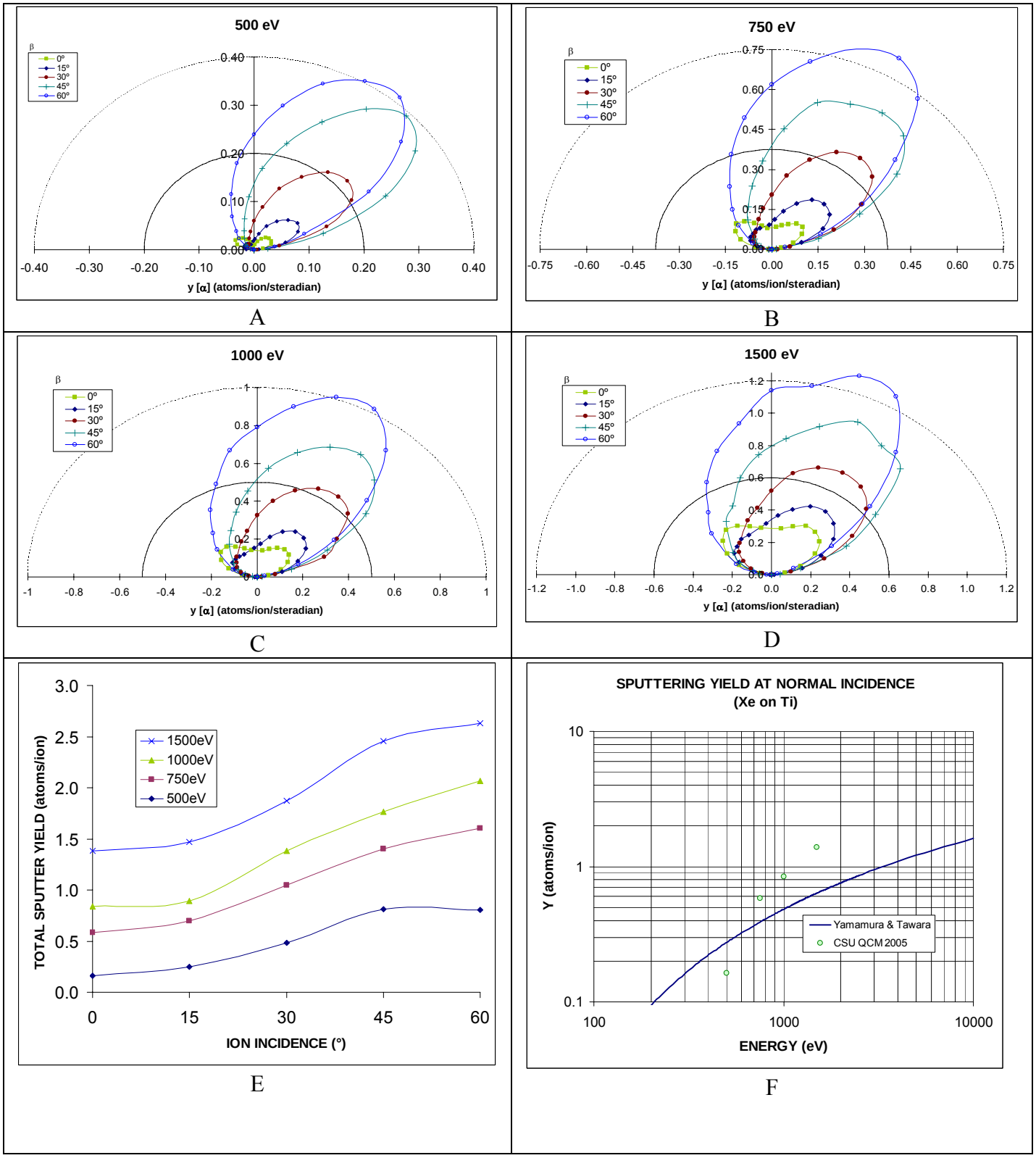

Figure 7. Results of Xenon ions on Titanium target

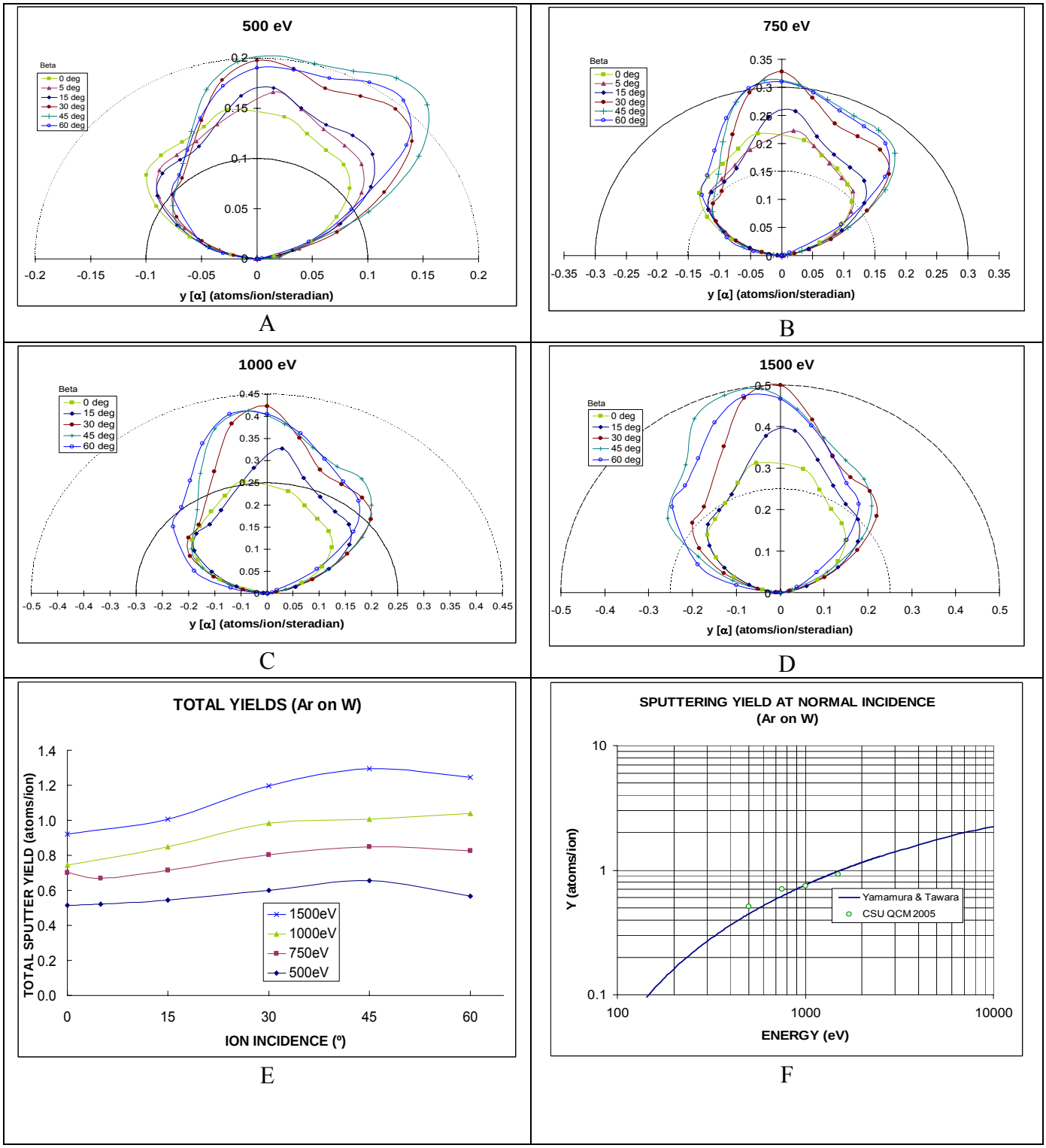

Figure 8. Results of Argon ions on Tungsten target

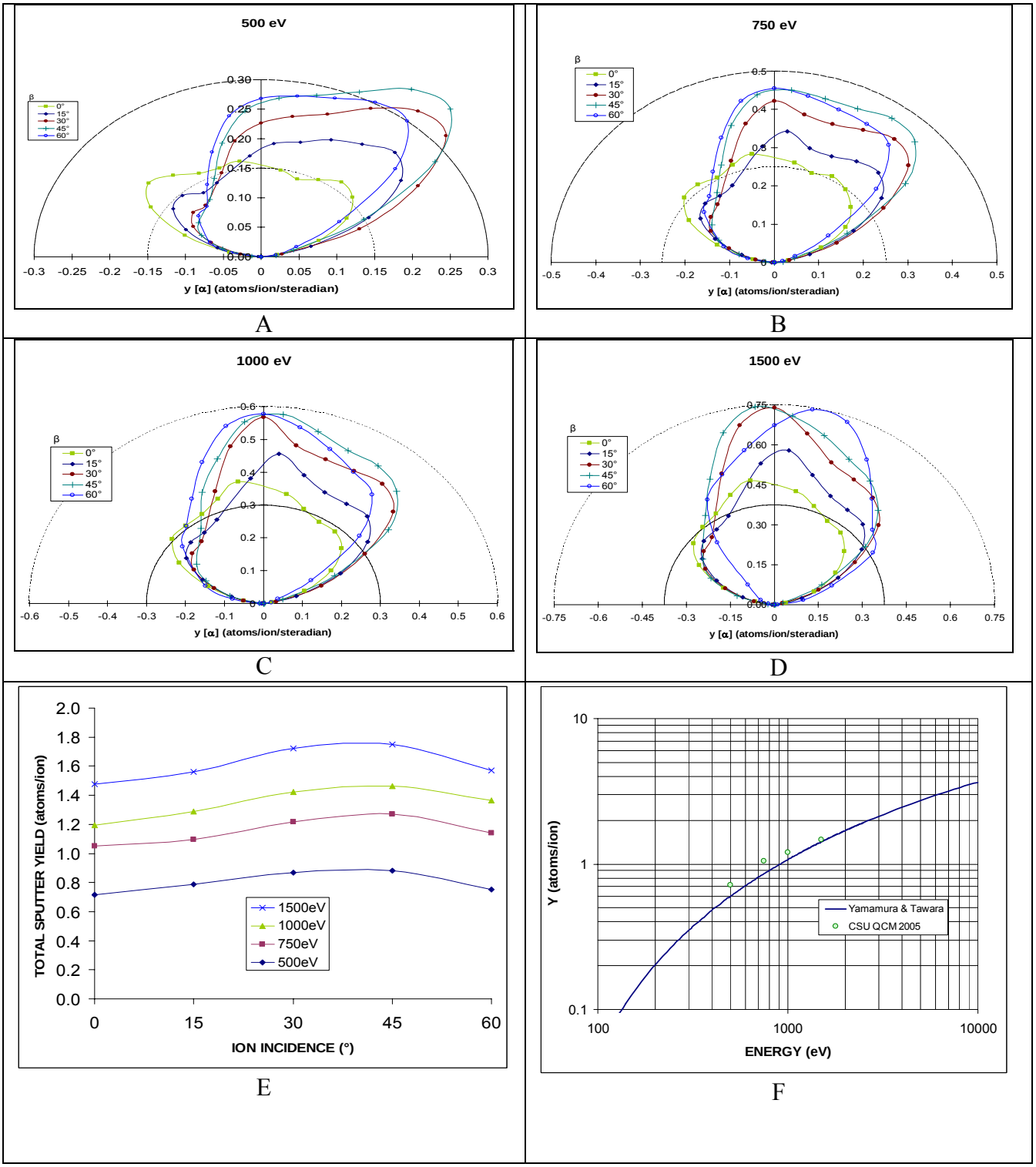

Figure 9. Results of Krypton ions on Tungsten target

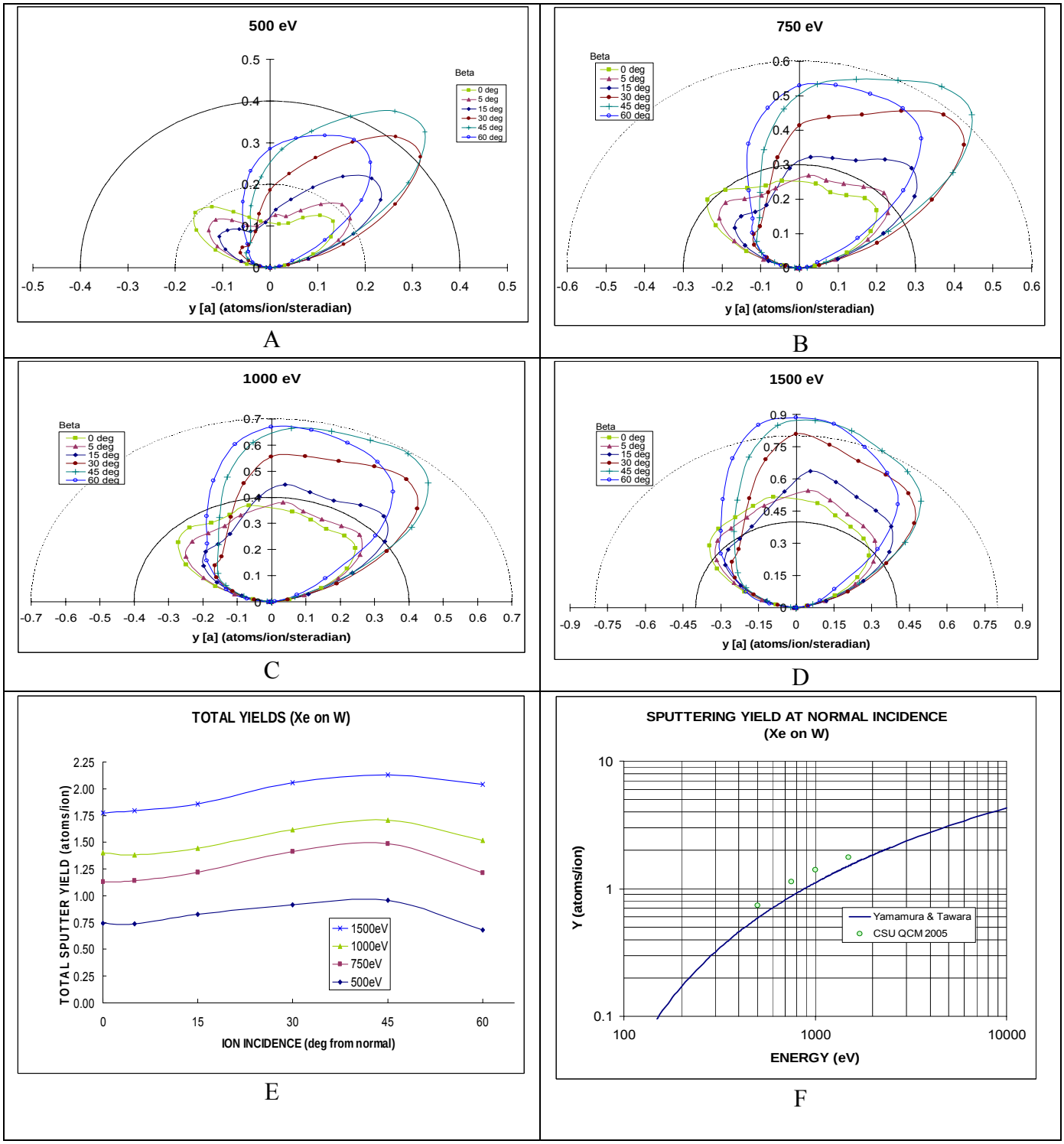

Figure 10. Results of Xenon ions on Tungsten target